

# Active Aeroelastic Control of the Supersonic Semispan Transport (S4T) Model

Kevin Roush<sup>\*</sup> Oddvar Bendiksen<sup>†</sup> Ross Gadien<sup>‡</sup>

Active aeroelastic control has the potential to address flutter, dynamic loads, and ride quality for supersonic transport configurations without adding weight, thereby enabling efficient high speed flight. In this development, control laws have been developed for a dynamically scaled wind tunnel model of a supersonic transport configuration known as the supersonic semispan transport (S4T). Control laws have been designed to simultaneously provide flutter suppression, gust load alleviation, and ride quality assurance to this configuration. These laws were developed using the Linear Quadratic Gaussian method with Loop Transfer Recovery. These control laws have been assessed using both analytical and experimental studies at the Transonic Dynamics Tunnel. Improvements in the aeroelastic response of the S4T are found in both analytical and experimental results.

## I. Introduction

The pursuit of increasingly advanced vehicles creates a demand for a strong capability for developing control laws to mitigate aeroelastic behavior. This demand is well exhibited through the example of high speed transport aircraft design. Significant study conducted during the NASA High Speed Research (HSR) program identified the importance of performing active control for flutter suppression, gust load alleviation, and ride quality enhancement<sup>1,2</sup>. These requirements apply across the transonic flight regime, making the problem significantly more challenging<sup>3,4,5</sup>.

In the 1990s, research was conducted under the High Speed Civil Transport (HSCT) program with the objective to develop affordable supersonic flight for the public<sup>6</sup>. The research under this program led to the Technology Concept Aircraft (TCA) configuration. Research of the TCA identified aeroelastic research as an important priority<sup>3</sup>. Several wind tunnel models were created including the Rigid Semispan Model (RSM)<sup>7</sup> and Flexible Semispan Model (FSM)<sup>8, 9</sup>. The flexible semispan model was used for open-loop aeroservoelastic testing, and numerous investigations were conducted on the behavior of this model including nonlinear and wavelet analyses conducted by Hajj et al.<sup>10, 11</sup>. The most recent aeroelastic model based on the HSCT is the Supersonic Semispan Transport (S4T)<sup>12</sup>. This model is a dynamically scaled version of the TCA<sup>1</sup> and is constructed with 43 embedded accelerometers and 3 hydraulically actuated control surfaces<sup>12</sup> (Figure 1, Figure 2). This model is used for the experimental demonstration of this research.

Active aeroelastic control has long been a research topic of interest. In fact, the use of active aeroelastic control for load alleviation and improved fatigue life dates back to the development of stability augmentation systems (SAS) for the XB-70<sup>13</sup> and B-52<sup>14</sup> in the late 1960s and early 1970s. Active flutter suppression methods have been researched since as early as 1971 by Nissim<sup>15</sup>. In the late 1970s active flutter suppression techniques were developed and demonstrated for wing/store flutter of a wind tunnel model representing the YF-17 fighter configuration<sup>16</sup>. The use of active controls on the YF-17 wind tunnel model led to stable behavior at 170% the open loop flutter dynamic pressure<sup>17</sup>. In the late 1980s and early 1990s active flutter suppression and load alleviation were developed for a fighter configuration based on the YF-17 known as the Active Flexible Wing (AFW)<sup>18</sup>. Control law development approaches applied to the AFW include classical control law design using root locus techniques<sup>19</sup> and multi-input/multi-output control for simultaneous flutter suppression and maneuver load reduction<sup>20</sup>. Application of the linear quadratic Gaussian (LQG) control design method to the AFW resulted in a 23% increase in flutter dynamic pressure<sup>21</sup>.

---

<sup>\*</sup> Vice President of Engineering, M4 Engineering. Member, AIAA.

<sup>†</sup> Professor, Department of Mechanical and Aerospace Engineering, University of California, Los Angeles, CA. Associate Fellow, AIAA.

<sup>‡</sup> Engineer, The Boeing Company. Senior Member, AIAA.



Figure 1. S4T model

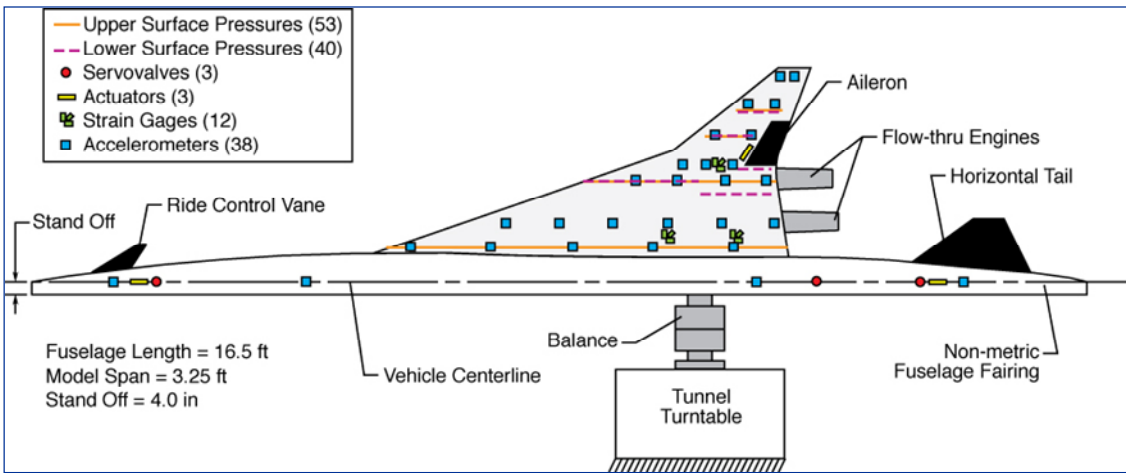


Figure 2. Location of sensors and control surfaces [22]

## II. Technical Approach

### A. Aeroservoelastic Plant Model Development

The aeroservoelastic plant model is developed based on representations of the structural dynamic and unsteady aerodynamic behavior of the S4T model. The structural dynamic behavior is characterized by a Nastran Finite Element Model (FEM) representing the mass and stiffness of the model. The first four flexible modes predicted by the FEM are shown in Figure 3. The frequencies of the first four modes have been tuned to match the structural frequencies measured in ground vibration test. The unsteady aerodynamic behavior of the S4T is characterized using the Doublet-Lattice Method<sup>23</sup>, Navier-Stokes CFD based reduced order models<sup>24</sup>, and Zona51 supersonic lifting surface theory<sup>25</sup> are used for the subsonic, transonic, and supersonic regimes respectively. Navier-Stokes results for a transonic condition are shown in Figure 4. The structural and unsteady aerodynamic models are combined to form the aeroservoelastic plant model as described in Reference 26.

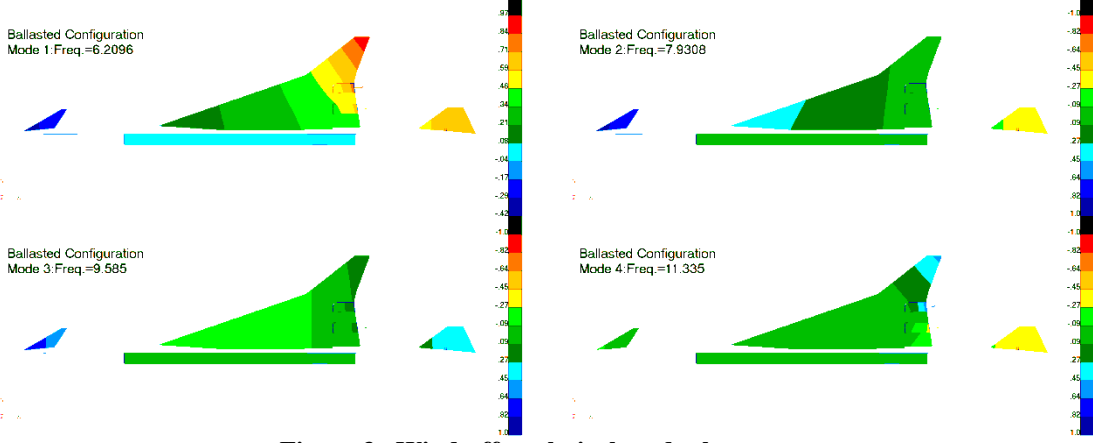


Figure 3. Wind-off analytical mode shapes

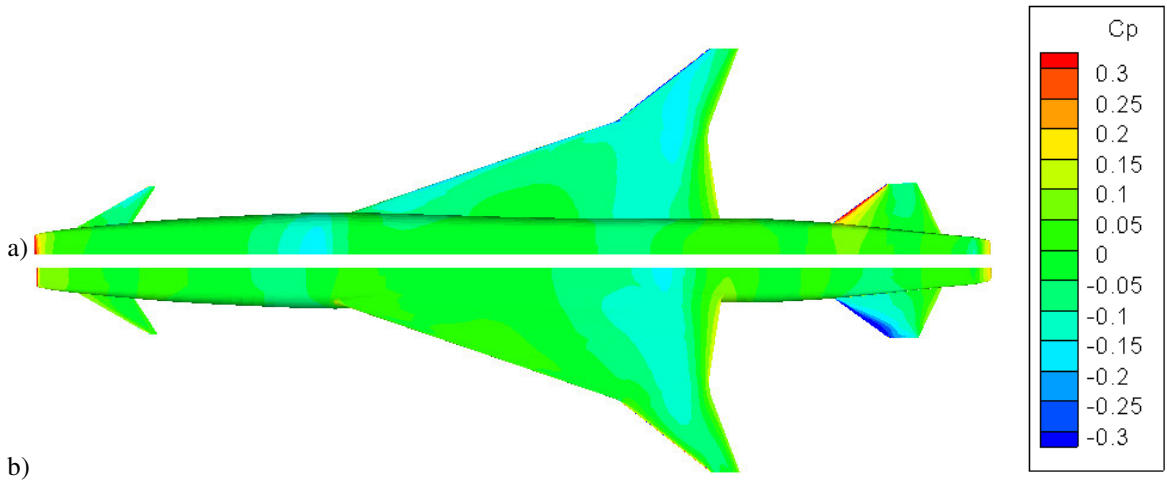


Figure 4. Surface pressure contours for a) upper and b) lower surface ( $M_{\infty}=0.95$ ) (Navier-Stokes).

### B. Control Law Design

We consider an LTI system in the form:

$$\begin{cases} \dot{x} = Ax + Bu \\ y = Cx + Du \end{cases} \quad (1)$$

where  $x \in \mathbb{R}^n$  is the  $n$ -dimensional state vector,  $u \in \mathbb{R}^m$  is the  $m$ -dimensional vector of controls, and  $y \in \mathbb{R}^p$  is the  $p$ -dimensional vector of measured outputs. Moreover, we assume that the matrix pair  $(A, B)$  is stabilizable and that the matrix pair  $(A, C)$  is observable. If the full state vector is available, state feedback control may be designed via Linear Quadratic Regulator (LQR) design to yield optimal solution:

$$u = -Kx \quad (2)$$

where  $K$  is the corresponding optimal feedback gain matrix.

Often the state vector is not available on-line, so in order to attain good stability margins and desired regulator performance, Linear Quadratic Gaussian (LQG) design with Loop Transfer Recovery (LTR) methodology<sup>27, 28, 29</sup> is utilized to control the desired regulated states. The rationale for using the LQG/LTR approach is that the method provides rigorous and consistent design steps in calculating optimal *output* feedback control solution using only available measurements. The LQG design process forms state observer

$$\hat{x} = A\hat{x} + Bu + L^T(\hat{y} - y) \quad (3)$$

with optimal Kalman gain matrix  $L$  constructed using available free design parameters and LQR feedback matrix  $K$  to form control signal based on the observer state:

$$u = -K\hat{x} \quad (4)$$

The Kalman gain is selected via the LTR process to recover the robustness properties of the full state feedback solution at either the plant input or output.

All of the controllers designed in this work were designed at dynamic pressures beyond the open-loop flutter boundary. The weighting matrices used in the LQR and LQG/LTR design process were chosen to achieve robustness for dynamic pressures ranging from wind-off to beyond the open-loop flutter boundary. Robustness evaluation was based on the minimum singular values of the return difference matrix<sup>30, 31, 32</sup>.

### C. Control Law Design Trade Studies

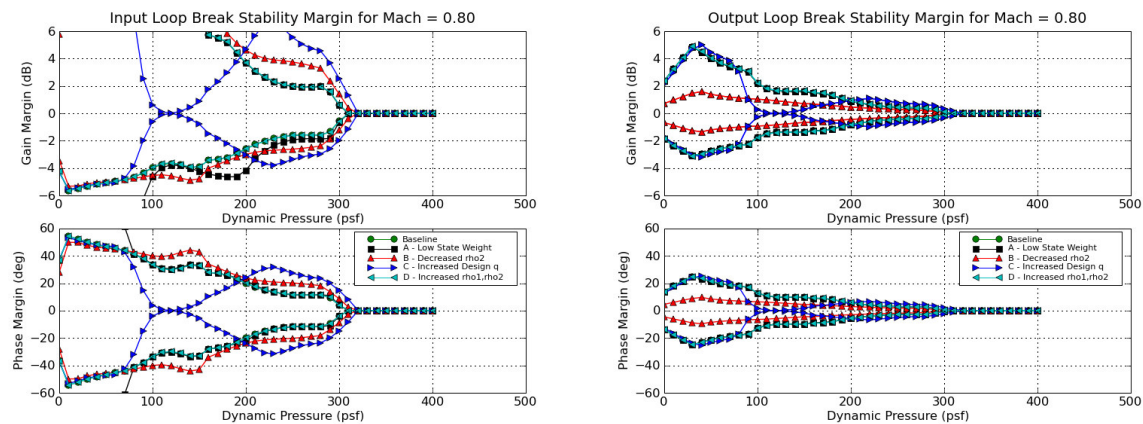
#### 1. Initial Design Study

A control design trade study was conducted to establish the sensitivity of the controller to variations in the design parameters, and indicate a favorable choice of parameters for use in design. This study was conducted for the ballasted configuration operating at Mach 0.80. The first variant in the design study made use of a limiting property of the LQR process described in Reference 27 as follows, “As state weighting goes to zero, the closed loop poles approach the stable open loop poles or the reflections through the  $j\omega$ -axis of the unstable poles.” Three more variants to the control design were considered including: decreased sensor noise weighting, increased design dynamic pressure, and increased estimator weighting. The design parameters associated with each controller in the trade study are shown in Table 1.

| Flight/Mass Condition                              | M=0.80<br>Ballasted | M=0.80<br>Ballasted     | M=0.80<br>Ballasted                  | M=0.80<br>Ballasted                   | M=0.80<br>Ballasted               |
|--|---------------------|-------------------------|--------------------------------------|---------------------------------------|-----------------------------------|
| Design Option                                      | Baseline            | A - Low state weighting | B – Decreased sensor noise weighting | C – Increased design dynamic pressure | D – Increased estimator weighting |
| State weighting of unstable modes ( $q_1$ )        | 8                   | 0.0001                  | 8                                    | 8                                     | 8                                 |
| State weighting of stable modes ( $q_2$ )          | 0                   | 0.0001                  | 0                                    | 0                                     | 0                                 |
| Control weighting ( $r$ )                          | 1                   | 1                       | 1                                    | 1                                     | 1                                 |
| Process noise intensity weighting ( $\rho_1$ )     | 0.1                 | 0.1                     | 0.1                                  | 0.1                                   | 1                                 |
| Measurement noise intensity weighting ( $\rho_2$ ) | 10                  | 10                      | 0.1                                  | 10                                    | 100                               |
| Design dynamic pressure (psf)                      | 150                 | 150                     | 150                                  | 225                                   | 150                               |

Table 1. Controller design parameters in trade study

Each of the controllers in the trade studies was designed at the prescribed dynamic pressure and evaluated across a range of dynamic pressures. The results are shown in Figure 5.



a)

b)

Figure 5. Gain and phase margin for (a) input loop break and (b) output loop break for initial control design trade study

The effect of design dynamic pressure can clearly be seen in the comparison of results. As expected, the controller designed at 225 psf has superior robustness to the controller designed at 150 psf for all conditions above 225 psf. At all conditions below 225, the controller designed for 150 psf demonstrates superior robustness. In fact, the controller designed at 225 psf input loop break gain margin drops to 0.12 dB at 110 psf. This provides an indication that the use of gain scheduling could provide increased margins across the range of dynamic pressures. If gain scheduling is not used, 150 psf is observed to be an acceptable choice of design dynamic pressure due to the lack of significantly decreased margins below the design pressure.

The results from the controller with low state weighing show an interesting behavior. For the dynamic pressures at which the open loop system is stable, the margins of the controller designed with low state weighting increase dramatically. At all dynamic pressures below the open loop flutter speed, this controller creates a system with input margins approaching or exceeding those guaranteed for a state feedback system (gain margin  $[1/2, \infty]$ , phase margin  $[-60^\circ, 60^\circ]$  [Ref 27]). At dynamic pressure beyond the open loop flutter pressure, the controller with low state weighting demonstrates margins at least equal to those of the baseline design, including increased negative gain margin for input loop break. Due to the increased stability margins, design using low state weighting is selected for future studies.

Decreased measurement noise intensity weighting results in increased margins for the input loop break case and decreased margins for the output loop break case. This result is to be expected as it indicates that the designs based on an assumption of lower sensor noise are less robust when the calculation is performed with the loop broken at the location of the sensor. The selection of noise intensity weighting matrix scale factors thus represents a significant design trade and is investigated further a subsequent trade study.

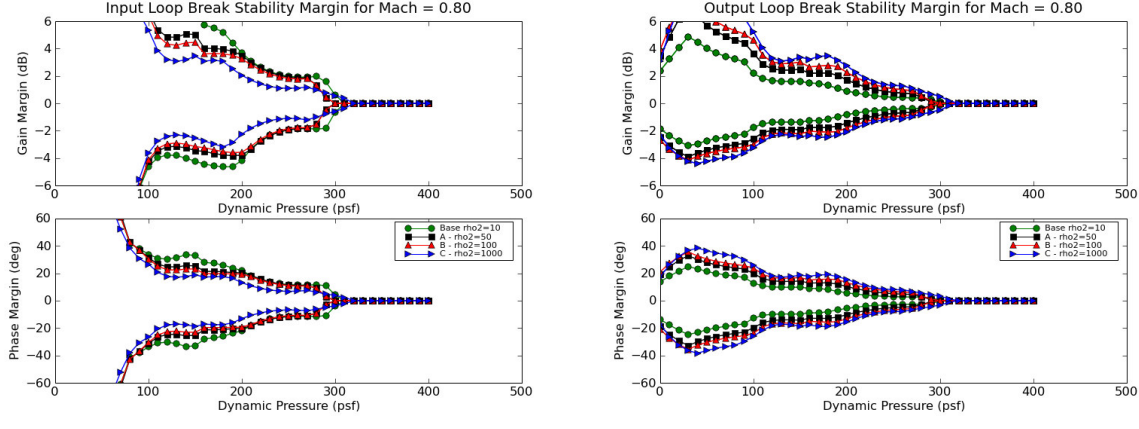
## 2. Estimator Design Trade Study

The results of the first design study resulted in the selection of low state weighting and a design dynamic pressure of 150 psf. A second study was conducted to further characterize the effect of scale factors chosen for the noise intensity weighting matrix. The design parameters associated with each controller in the trade study are shown in Table 2.

| Flight/Mass Condition                                 | M=0.80<br>Ballasted     | M=0.80<br>Ballasted | M=0.80<br>Ballasted | M=0.80<br>Ballasted |
|---|-------------------------|---------------------|---------------------|---------------------|
| Design Option   | Baseline<br>$\rho_2=10$ | $A - \rho_2=50$     | $B - \rho_2=100$    | $C - \rho_2=1000$   |
| State weighting of all modes (q)                      | 0.0001                  | 0.0001              | 0.0001              | 0.0001              |
| Control weighting (r)                                 | 1                       | 1                   | 1                   | 1                   |
| Process noise intensity weighting ( $\rho_1$ )        | 0.1                     | 0.1                 | 0.1                 | 0.1                 |
| Measurement noise intensity<br>weighting ( $\rho_2$ ) | 10                      | 50                  | 100                 | 1000                |
| Design dynamic pressure (psf)                         | 150                     | 150                 | 150                 | 150                 |

**Table 2. Controller design parameters in trade study**

Each of the controllers in the trade studies was designed at the prescribed dynamic pressure and evaluated across a range of dynamic pressures. The results are shown in Figure 6. The results extend the same trend as seen in the initial study to higher values of the sensor noise weighting matrix. Selection among the results in this trade study should be based on the relative expectation of noise, nonlinearity, and inaccuracy at the input and output of the plant. The controller based on a sensor noise weight of 50 is currently selected. For that controller, the input loop break gain margin is -3.5 to 4.4 dB and phase margin is  $+/ - 23^\circ$  at two times the open loop flutter dynamic pressure (156 psf). For the controller with a sensor noise weighting of 10, the input loop break margins are at least -3.8 to 6.4 dB and  $+/ - 30^\circ$  at all dynamic pressures below 156 psf.



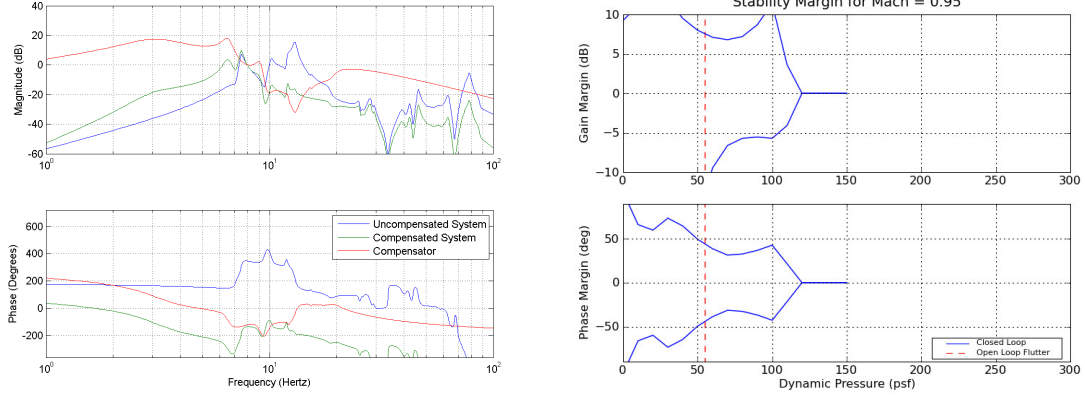
a)

b)

**Figure 6. Gain and phase margin for (a) input loop break and (b) output loop break for sensor noise control design trade study**

### III. Analytical Results

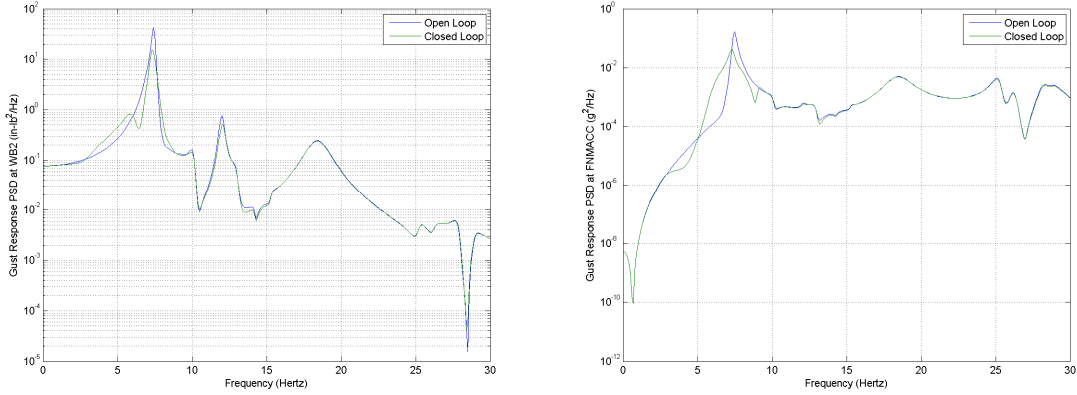
Simulations were performed for controllers designed at subsonic, transonic, and supersonic ( $M=0.80, 0.95, 1.10$ ) conditions. The open and closed loop response of wing strain gages and fuselage accelerometers were simulated as indications of gust loads and passenger station ride accelerations respectively. Gain and phase margins were calculated for a range of dynamic pressures. Figure 7 shows simulation results at the transonic condition with closed loop flutter occurring at over 200% of open-loop flutter. Figure 8 and Figure 9 show reductions of over 20% in gust loads and ride accelerations at dynamic pressures of 70% of the open-loop flutter boundary and above.



a)

b)

**Figure 7. Analytical results at  $M=0.95$  showing a) controller transfer function b) robustness margins.**



a)

b)

**Figure 8. Analytical results at  $M=0.95$  showing a) gust load alleviation at  $q=60\text{psf}$  b) ride quality assurance at  $q=60\text{psf}$**

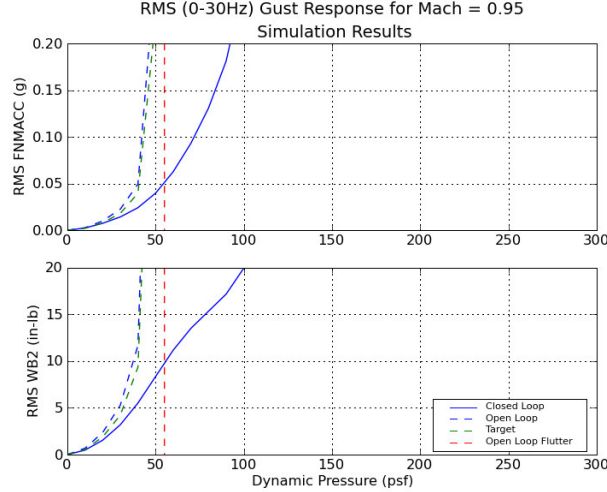


**Figure 9. Gust load alleviation and ride quality assurance at  $M=0.95$  at a range of dynamic pressures.**

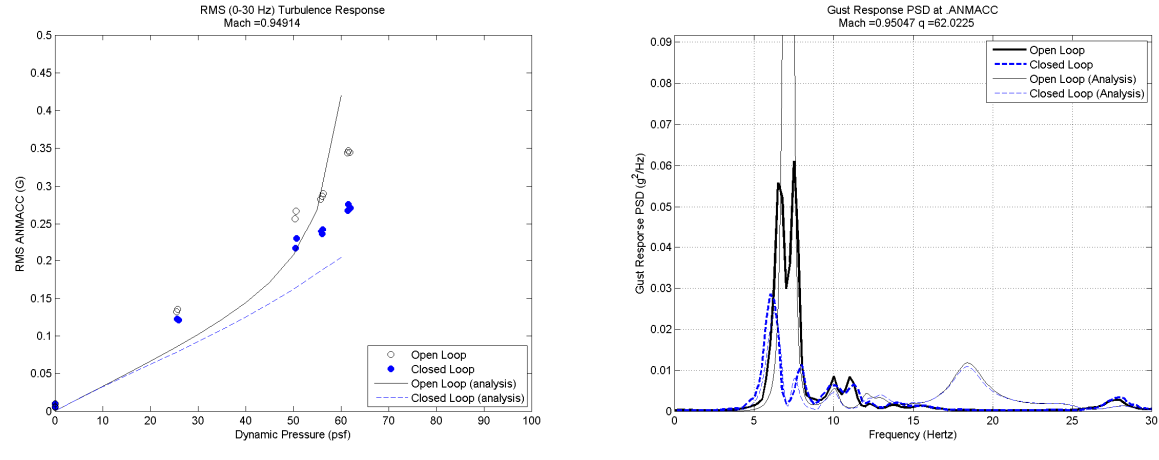
#### IV. Experimental Results

Closed loop wind tunnel testing was conducted at NASA Langley in the summer of 2009. Testing was conducted for three Mach numbers ( $M_\infty=0.80, 0.95, 1.10$ ) at various dynamic pressures below the open loop flutter dynamic pressure. The experimental data was processed to evaluate the effectiveness of the ride quality assurance, gust load alleviation, and flutter suppression functions of the control laws. These results along with comparisons to analytical predictions are discussed in the following subsections.

##### A. Ride Quality Assurance

The ride quality function of the control laws is evaluated at forward and aft locations on the fuselage. The RMS vibration in the aeroelastic frequency band is calculated by taking the square root of the acceleration PSD function integrated from 0 to 30 Hz. Aft fuselage vibration RMS levels from analysis and test are compared in Figure 10a. Except for the case of high dynamic pressure and open loop, the analysis data is generally below the test data by approximately 20%. Possible reasons for this include noise in the test data, differences in the simulated and actual turbulence spectrum, and differences in the analysis and test mode shapes. The open loop data simulation exhibits a significant increase at high dynamic pressure. Figure 10b shows that for high dynamic pressures, the critical open loop peaks have significantly higher amplitude than the test data. A likely reason for this is nonlinearity in the system that limits the motion for high amplitudes. The closed loop data exhibits a relatively good match between test and analysis. The closed loop RMS vibration is 20% lower than the closed loop case for the transonic condition indicating that the control law is effective at reducing the vibration at the aft fuselage.

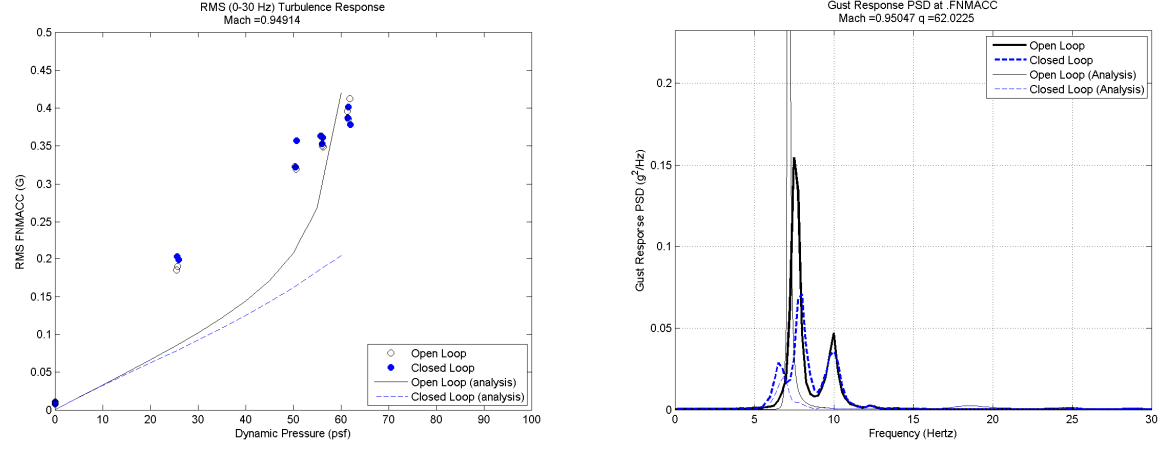
Forward vibration RMS levels are shown in Figure 11a. This data exhibits a similar behavior to that at the aft fuselage for open loop cases at high dynamic pressure. The forward fuselage data also shows an underprediction of the vibration levels by about 50% RMS. This is likely due to the reasons mentioned above. The results also show that while no reduction is present in the test data, it is clearly present in the analysis. This is likely due to discrepancies between the analytical model and the actual system that are more pronounced for sensors located further from the actuation location. The PSD results are compared in Figure 11b and indicate that while the experimental data shows a suppression of the second mode, it is significantly less pronounced than that seen in the analytical model.



a)

b)

**Figure 10. Comparison of transonic analysis and test acceleration results for aft fuselage acceleration: (a) RMS 0-30 hz at multiple flight conditions, (b) PSD at maximum dynamic pressure.**



a)

b)

**Figure 11. Comparison of transonic analysis and test acceleration results for forward fuselage acceleration: (a) RMS 0-30 hz at multiple flight conditions, (b) PSD at maximum dynamic pressure.**

## B. Gust Load Alleviation

Wing loads are calculated via a linear combination of strain gage data. The gust load alleviation function of the control laws is evaluated by investigation of wing root bending moment. The RMS moment in the aeroelastic frequency band is calculated by taking the square root of the acceleration PSD function integrated from 0 to 30 Hz. Analysis-test comparisons for bending moment data are shown in Figure 12. The analytical model underpredicts the test data by approximately 80%. This is significantly more than for the acceleration data. Investigation of the PSD data at high dynamic pressure (Figure 13) indicates that while the first mode (bending branch) is critical in the analysis, the second mode (torsion branch) is critical in the test data. This can be seen clearly in Figure 13a where

the peak in the analytical open loop data is at 7.2 Hz and the peak in the test open loop data is at 6.5 Hz. A possible cause of this would be inaccuracy of the analytical mode shapes. While the SISO control laws suppress the second mode, they exacerbate the first mode and do not accomplish gust load alleviation. The MIMO control law which includes the aileron achieves 6% reduction in the RMS wing bending moment (Figure 12b).

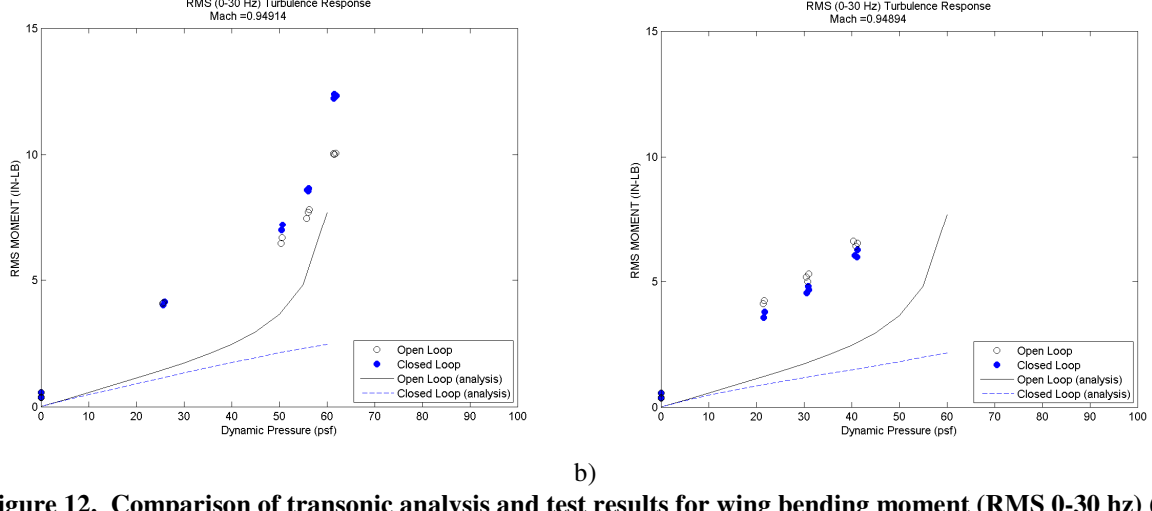


**Figure 12. Comparison of transonic analysis and test results for wing bending moment (RMS 0-30 hz) (a) SISO, (b) MIMO.**

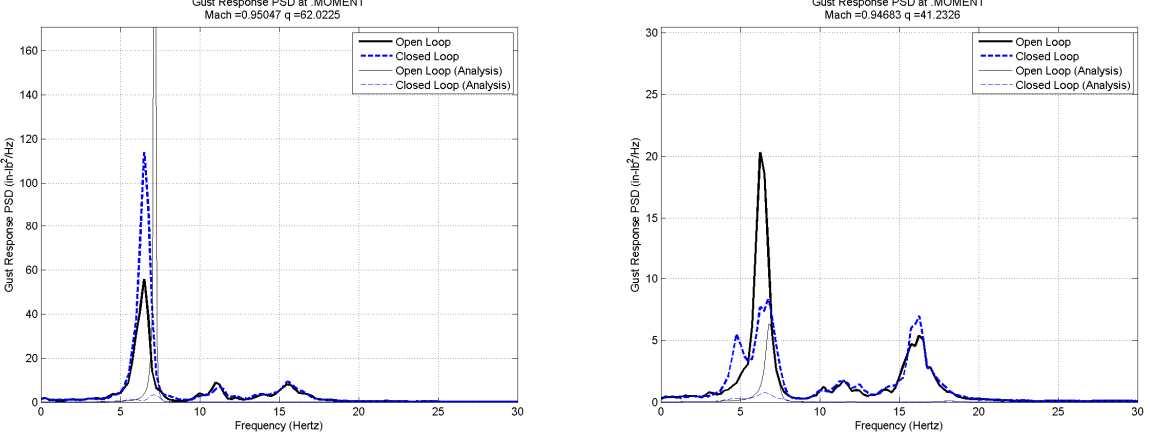


**Figure 13. Comparison of transonic analysis and test results for wing bending moment PSD (a) SISO, (b) MIMO.**

### C. Flutter Suppression

The effectiveness of the control laws in achieving flutter suppression is determined through the use of the Zimmerman-Weissenburger method. The Zimmerman-Weissenburger method is named after the authors of a 1964 paper documenting the method<sup>33</sup>. The authors present a linear two degree of freedom flutter system. Based on the Routh stability criteria<sup>34</sup> of this system, a flutter margin is calculated using:

$$F = \left[ \frac{\omega_2^2 - \omega_1^2}{2} + \frac{\beta_2^2 - \beta_1^2}{2} \right]^2 + 4\beta_1\beta_2 \left[ \frac{\omega_2^2 + \omega_1^2}{2} + 2 \left( \frac{\beta_2 + \beta_1}{2} \right)^2 \right] - \left[ \left( \frac{\beta_2 - \beta_1}{\beta_2 + \beta_1} \right) \left( \frac{\omega_2^2 - \omega_1^2}{2} \right) + 2 \left( \frac{\beta_2 + \beta_1}{2} \right)^2 \right]^2 \quad (5)$$

where  $\omega_1$  and  $\omega_2$  are the frequencies of the first two modes and  $\beta_1$  and  $\beta_2$  are the decay rates for the first two modes. For the case of a linear, two degree of freedom aeroelastic system, flutter occurs when the flutter margin is equal to zero. The authors show application of this method with linear and quadratic extrapolations of subcritical data points

for predicting the flutter speed of various multi degree of freedom systems. For application to the aeroelastic system in this work, the frequency and damping of the critical modes are taken from the identified four-state models described above.

The modal frequency results for the transonic case are plotted as a function of dynamic pressure in Figure 14a. In the open loop case, the frequency of the second mode decreases with increasing dynamic pressure while the frequency of the first mode increases. In the closed loop case, the frequency of the second mode actually increases with increasing dynamic pressure resulting in negligible coalescence of the modal frequencies. The Zimmerman-Weissenburger flutter margin results (Figure 14b) show the effects of this frequency behavior with the predicted flutter speed for the closed loop system 75% higher than that for the open loop system. Note that while the open loop data is well fit by a linear function, the closed loop data appears to exhibit a concave trend. If the closed loop data is fit with a quadratic function, the predicted flutter suppression effectiveness is greater than the 75% predicted based on a linear curve fit.

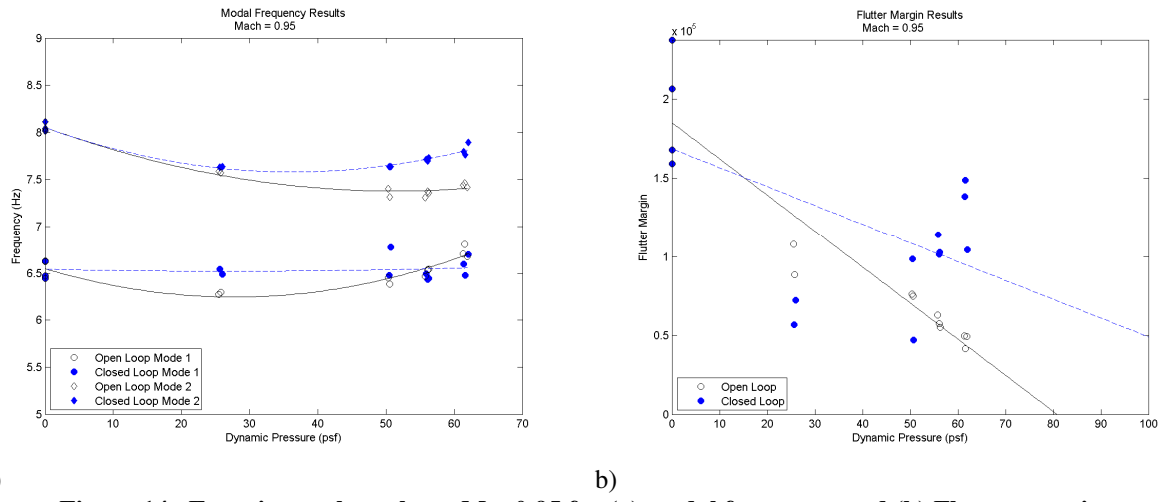


Figure 14. Experimental results at  $M_\infty=0.95$  for (a) modal frequency and (b) Flutter margin.

## V. Conclusion

Predicted and measured values for ride quality assurance, gust load alleviation, and flutter suppression have been computed for four control laws tested at the TDT. These control laws were developed based on analytical models tuned based on stiffness, mass, and wind-off vibration data and were able to provide active aeroelastic control to the S4T model. Aft fuselage RMS vibration reduction of greater than 20% was achieved at the aft fuselage for all Mach numbers tested. The GLA controller tested achieved 11% reduction in RMS shear and 6% reduction in bending moment. It is expected that slight modification to the design of this control law could create robustness at higher dynamic pressures resulting in higher GLA. Increased spacing of the critical modes was achieved at all Mach numbers tested. Flutter dynamic pressures calculated based on the Zimmerman-Weissenburger method and indicate that flutter dynamic pressure increases of 21%, 75%, and 32% were achieved for the subsonic, transonic, and supersonic cases respectively.

| Mach Number | Dynamic Pressure Range | Type     | Fuselage Vibration Reduction (%) |     | Wing Gust Load Reduction (%) |       | Flutter Speed Increase (%) |
|-------------|------------------------|----------|----------------------------------|-----|------------------------------|-------|----------------------------|
|             |                        |          | Forward                          | Aft | Moment                       | Shear |                            |
| 0.80        | 0-65 psf               | SISO-FSS | 13                               | 23  | N/A                          | 7     | 10                         |
| 0.95        | 0-62 psf               | SISO-FSS | 1                                | 20  | N/A                          | 13    | 32                         |
| 1.10        | 0-65 psf               | SISO-FSS | N/A                              | 27  | N/A                          | 19    | 15                         |
| 0.95        | 0-41 psf               | MIMO-GLA | 2                                | 16  | 6                            | 11    | N/A                        |

Table 3. Summary of Experimental Results

## VI. Acknowledgement

Funding for this development has been provided by the Aeroelasticity Branch at NASA Langley Research Center. The technical monitor is Boyd Perry. All experimental work was performed by NASA at the Transonic Dynamics Tunnel with support from M4 Engineering and Zona Technology.

## VII. References

1. Baker, M. L. and Lenkey, P. W. *Parametric Flutter Analysis of the TCA Configuration and Recommendation for FFM Design and Scaling*, McDonnell Douglas Report CRAD-9306-TR-3088
2. Fogarty, T., and Baker, M. L. *MSC/NASTRAN Flutter Analysis of TCA with Lateral and Directional Control Laws*, 6/30/1998. HSR Program memorandum
3. Baker, M.L., Mendoza, R., and Hartwich, P.M. "Transonic Aeroelastic Analysis of a High Speed Transport Wind Tunnel Model," AIAA-99-1217, AIAA/ASME/ASCE/AHS/ASC Structures, Structural Dynamics, and Materials Conference and Exhibit, 40th, St. Louis, MO, Apr. 12-15, 1999.
4. Bendiksen, Oddvar O, "Transonic Flutter," 43rd AIAA Structures, Structural Dynamics, and Materials Conference, Denver, CO, April 22-25, 2002. pp. pp. 273-286.
5. Bendiksen, Oddvar O, "Role of Shock Dynamics in Transonic Flutter," AIAA Dynamics Specialists Conference, Dallas, TX, Apr. 1992. pp. pp. 401-414.
6. Welge, R. H. "Douglas Aircraft HSCT Status and Future Research Needs," Langley Research Center, First Annual High-Speed Research Workshop, 1992.
7. Scott, R. C., Silva, W. A., Florance, J. R., and Keller, D. F. "Measurement of Unsteady Pressure Data on a Large HSCT Semispan Wing and Comparison with Analysis," 2002-1648, 43rd AIAA/ASME/ASCE/AHS/ASC Structures, Structural Dynamics, and Materials Conference, Denver, CO, 2002.
8. Baker, M. L., Mendoza, R., and Hartwich, P. M. "Transonic Aeroelastic Analysis of a High Speed Transport Wind Tunnel Model," 1999-1217, AIAA/ASME/ASCE/AHS/ASC Structures, Structural Dynamics, and Materials Conference and Exhibit, 40th, St. Louis, MO, 1999.
9. Schuster, D. M., Spain, C. V., Turnock, D. L., Rausch, R. D., Hamouda, M-N., Vogler, W. A., and Stockwell, A. E. "Development, Analysis and Testing of the High Speed Research Flexible Semispan Model," STAR, Vol. 37, No. 8, 1999.
10. Chabalko, C. C., Hajj, M. R., and Silva, W. A. ""Flutter of High-Speed Civil Transport Flexible Semispan Model: Time-Frequency Analysis", " *Journal of Aircraft*, Vol. 43, No. 3, 2006, pp. 743-748.
11. Hajj, M. R., and Silva, W. A. ""Nonlinear Flutter Aspects of the Flexible HSCT Semispan Model", " *Journal of Aircraft*, Vol. 41, No. 5, 2004, pp. 1202-1208.
12. Perry B., Silva W., Florance J., Wieseman C., Pototsky A., Sanetrik M., Scott R., Keller D., and Cole S. "Plans and Status of Wind-Tunnel Testing Employing an Aerostervoelastic Semispan Model," 48th AIAA/ASME/ASCE/AHS/ASC Structures, Structural Dynamics, and Materials Conference, Honolulu, HI, April 2007.
13. Lock, W., Kordes, E., McKay, J., and Wykes, J. *Flight Investigation of a Structural Mode Control System for the XB-70 Aircraft*, Oct 1, 1973. NASA-TN-D-7420
14. Dempster, J., and Roger, K. "Evaluation of B-52 Structural Response," *Journal of Aircraft*, Vol. 4, No. 6, 1967.
15. Nissim, E. *Flutter Suppression Using Active Controls Based on the Concept of Aerodynamic Energy*, March 1971. NASA TN D-6199
16. Advisory Group for Aerospace Research and Development, "Report on a Cooperative Programme on Active Flutter Suppression," Athens, Apr. 1980.
17. Hwang, C., Johnson, E.H., and Pi, W.S. "Recent Development of the YF-17 Active Flutter Suppression System," AIAA, Structures, Structural Dynamics, and Materials Conference, 21st, Seattle, Washington, May 1980.
18. Perry, B. III, Cole, S. R., and Miller, G. D. "Summary of an Active Flexible Wing Program," *Journal of Aircraft*, Vol. 32, No. 1, Jan.-Feb. 1995.
19. Waszak, M. R., and Srinathkumar, S. "Flutter Suppression for the Active Flexible Wing - A Classical Design," *Journal of Aircraft*, Vol. 32, No. 1, 1995.
20. Adams, W. M. Jr., and Christhilf, D. M. "Design and Multifunction Tests of a Frequency Domain-Based," *Journal of Aircraft*, Vol. 32, No. 1, 1995.
21. Mukhopadhyay, V. "Flutter Suppression Control Law Design and Testing for the Active Flexible Wing," *Journal of Aircraft*, Vol. 32, No. 1, 1995.
22. Florance, J. *Results from the Recent Aeroelastic Wind-Tunnel Test*, Hampton, VA : NASA, October 2007.

23. Giesing J. P., Kalman T.P., and Rodden W.P. "Subsonic unsteady aerodynamics for general configuration," AFFDL-TR-71-5, 1971.
24. Silva, W. A., and Bartels, R. E. "Development of Reduced-Order Models for Aeroelastic Analysis and Flutter Prediction Using the CFL3Dv6.0 Code," *Journal of Fluids and Structures*, Vol. 19, No. 6, July 2004, pp. 729-745.
25. Liu, D. D., Chen, P. C., Pototzky, A. S., and James, D. K. "Further Studies of Harmonic Gradient Method for Supersonic Aeroelastic Applications," *Journal of Aircraft*, Vol. 28, No. 9, 1991.
26. Roughen, K.M., Bendiksen, O.O., and Baker, M.L. "Development of Generalized Aeroseervoelastic Reduced Order Models," 50th AIAA Structures, Structural Dynamics, and Materials Conference, Palm Springs, CA, 2009.
27. Anderson, B. and Moore, J. *Optimal Control Linear Quadratic Methods*, Dover Publications, Inc., Mineola, New York, 2007.
28. Kalman, R. E., and Bucy, R. S. "New Results in Linear Filtering and Prediction Theory," *Trans. ASME Ser. D: J. Basic Eng.*, Vol. 83, 1961.
29. Doyle, J. C., and Stein, G. "Robustness with Observers," *IEEE Trans. Auto. Control*, Vols. AC-24, No. 4, 1979.
30. Macfarlane, A. G. J., and Postlethwaite, I. "The Generalized Nyquist Stability Criterion and Multivariable Root Loci," *International Journal of Control*, Vol. 25, 1977.
31. Safonov, M. G. and Athans, M. "A Multiloop Generalization of the Circle Criterion for Stability Margin Analysis," *IEEE Transactions on Automatic Control*, Vols. AC-26, 1981.
32. Gradient, R. and Lavretsky, E. *Control Design Guidelines*, Huntington Beach : The Boeing Company, 2008.
33. Zimmerman, N. H., and Weissenburger, J. T. "Prediction of Flutter Onset Speed Based on Flight Testing at Subcritical Speeds," *Journal of Aircraft*, Vol. 1, No. 4, 1964.
34. Routh, E. J. *Treatise on the Stability of a Given State of Motion*, 1877.